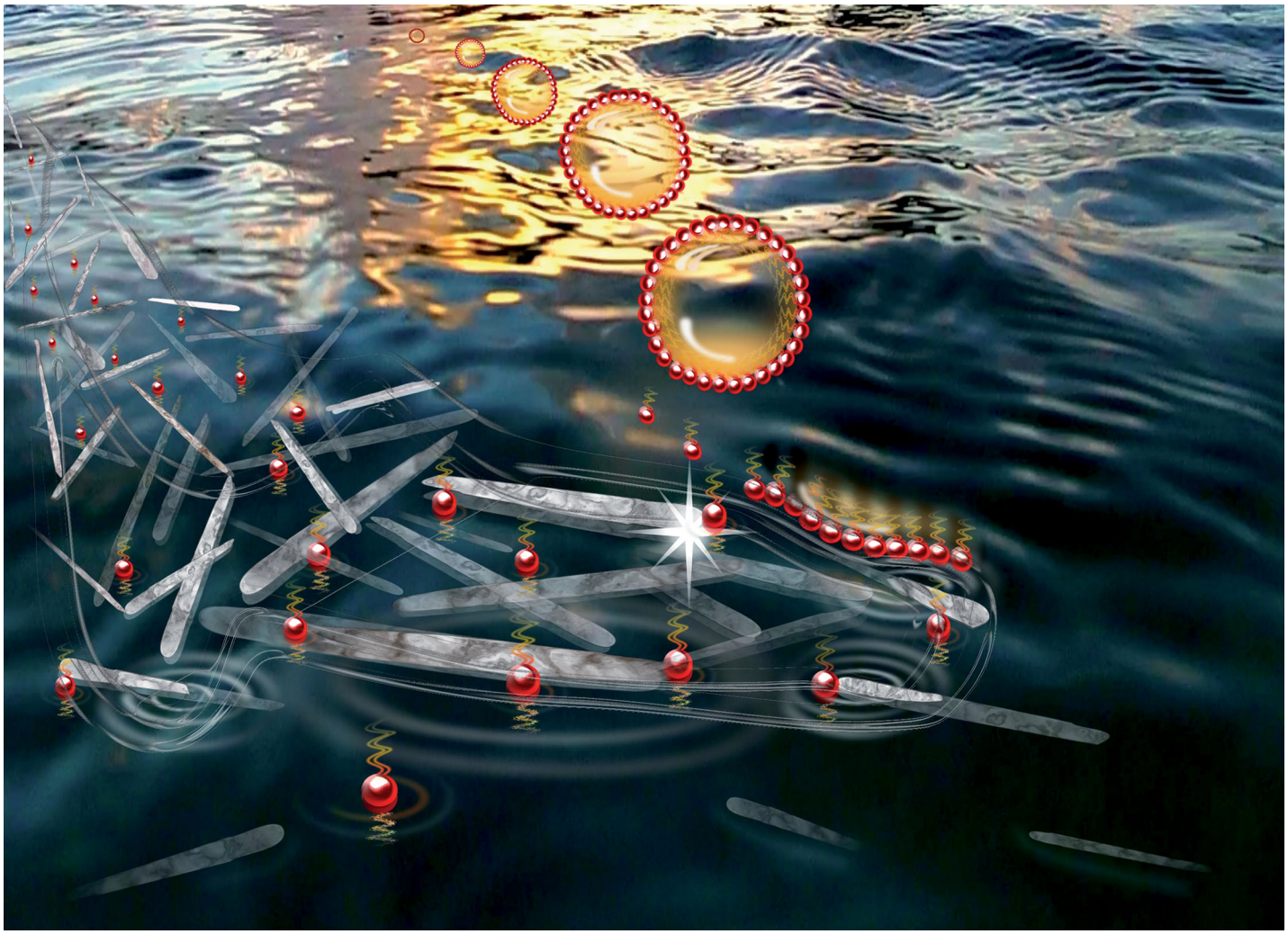

Research from the Edler group in the Department of Chemistry, University of Bath.

Charge-driven interfacial gelation of cellulose nanofibrils across the water/oil interface

Complexation of water-dispersible and negatively charged oxidised cellulose nanofibrils with an oil-soluble and positively charged surfactant, oleylamine, across the water/oil interface results in an interfacial gel, containing embedded oil droplets, resulting from spontaneous emulsification.

As featured in:

See Karen J. Edler *et al.*, *Soft Matter*, 2020, **16**, 357.

ROYAL SOCIETY OF CHEMISTRY

rsc.li/soft-matter-journal

Registered charity number: 207890

Soft Matter

PAPER

View Article Online
View Journal | View Issue

Cite this: *Soft Matter*, 2020, **16**, 357

Charge-driven interfacial gelation of cellulose nanofibrils across the water/oil interface†

Vincenzo Calabrese, [a] Marcelo A. da Silva, [a] Julien Schmitt, [a] Kazi M. Zakir Hossain, [a] Janet L. Scott [ab] and Karen J. Edler *[a]

Received 2nd August 2019,
Accepted 6th November 2019

DOI: 10.1039/c9sm01551e

rsc.li/soft-matter-journal

Interfacial gels, obtained by the interaction of water-dispersible oxidised cellulose nanofibrils (OCNF) and oil-soluble oleylamine (OA), were produced across water/oil (W/O) interfaces. Surface rheology experiments showed that the complexation relies on the charge coupling between the negatively-charged OCNF and OA. Complexation across the W/O interface was found to be dependent on the ζ-potential of the OCNF (modulated by electrolyte addition), leading to different interfacial properties. Spontaneous OCNF adsorption at the W/O interface occurred for particles with ζ-potential more negative than −30 mV, resulting in the formation of interfacial gels; whilst for particles with ζ-potential of *ca.* −30 mV, spontaneous adsorption occurred, coupled with augmented interfibrillar interactions, yielding stronger and tougher interfacial gels. On the contrary, charge neutralisation of OCNF (ζ-potential values more positive than −30 mV) did not allow spontaneous adsorption of OCNF at the W/O interface. In the case of favourable OCNF adsorption, the interfacial gel was found to embed oil-rich droplets – a spontaneous emulsification process.

Introduction

Over the last decade rod-like cellulose nanoparticles (CNP), such as cellulose nanofibrils (CNF) and cellulose nanocrystals (CNC), have received much attention due to the combined biocompatibility and tuneable self-assembly of these particles, which allows the production of eco-friendly materials with tailored properties.[1] The relationship between CNP assembly and bulk properties has been widely explored, through the combination of surface modification and tuning of environmental conditions (*e.g.*, pH,[2] ionic strength,[3,4] presence of surfactants,[5,6] and heat[7]). Stable CNP dispersions have been successfully produced by introducing charged moieties onto cellulose nanoparticle surfaces.[8] For example, oxidised cellulose nanofibrils (OCNF) produced *via* 2,2,6,6-tetramethylpiperidine-1-oxyl radical (TEMPO)-mediated oxidation of cellulose, bear carboxylate groups on the surface of the cellulose fibrils, allowing for negatively charged surfaces at appropriate pHs.[9–11] OCNF self-assembly has been found to be strongly dependent on electrostatic interfibrillar interactions; specifically, charge screening of the fibrils has been shown to be the main driving factor in enhancing interfibrillar interactions due to the associative forces outweighing repulsive charge interactions.[3,12]

CNP assembly across water/oil (W/O) interfaces has been broadly investigated in the context of Pickering emulsions, since CNP are good emulsion stabilizers.[13,14] The physicochemical properties of such emulsions are dictated by the coupled bulk (*e.g.*, droplet–droplet interactions) and W/O interfacial properties (*e.g.*, interfacial binding and rigidity). Although information regarding the bulk properties of emulsions can be obtained using several techniques (*e.g.*, rheology, scattering techniques), probing the interfacial properties of microscopic droplets can be a challenge. Due to this, the study of planar liquid–liquid interfaces *via*, for example, surface shear rheology or reflectometry, or of interfaces generated on macroscopic droplets (*e.g.*, *via* pendant drop tensiometric measurements) have been employed as model systems to yield insights into CNP assembly at the interface between two immiscible liquid phases. Recently, Bertsch *et al.* reported on the spontaneous adsorption of CNC at water/air (W/A) interface without the addition of any chemical modification or additional species (*e.g.*, surfactants).[15] In this field, three main approaches have been broadly employed to tune the wettability of CNP, favouring their adsorption to the interface: (i) electrostatic complexation between oppositely charged CNP and water-soluble amphiphilic species (*e.g.*, surfactants),[16–18] (ii) covalent hydrophobization of the CNP interface,[19–21] and, (iii) interfacial polyelectrolyte–CNP charge complexation between a polyelectrolyte, which is largely soluble in the organic phase (*e.g.*, oil),

[a] *Department of Chemistry, University of Bath, Claverton Down, Bath, BA2 7AY, UK. E-mail: k.edler@bath.ac.uk*
[b] *Centre for Sustainable Chemical Technologies, University of Bath, Claverton Down, Bath, BA2 7AY, UK*

† Electronic supplementary information (ESI) available: CMC of OA, strain sweep experiments, microscopy images, and further details on the interfacial shear rheology setup. See DOI: 10.1039/c9sm01551e

and an oppositely charged water-dispersible CNP. This last approach relies on the use of two immiscible liquids as scaffolds, delivering two oppositely-charged species and directing assembly across the liquid–liquid interface, analogously to the more extensively studied complex coacervates.[22,23] Recently, interfacial polyelectrolyte–CNP charge complexes, also called nanoparticle-surfactants,[24,25] have received great attention due to their synergistic effect in reducing surface tension across the liquid–liquid interface as well as their ability to form structured interfaces which allowed the production of capsules,[26] liquid tubules[27] and all-liquid objects.[28] In these systems, harnessing the 2D assembly of CNP across the immiscible phases is crucial for the formation of long-lived structures as well as to impart specific mechanical properties. On this ground, we have assessed the mechanical properties of the W/O interface upon complexation of negatively-charged water-dispersible CNP with an oppositely-charged oil-soluble species under conditions where bulk contributions are negligible, allowing exploration of the interfacial phenomena alone. A combination of surface shear rheology and microscopic analyses have been used to successfully probe the spontaneous interfacial complexation of the negatively charged OCNF with the oil-soluble and positively charged surfactant, oleylamine (OA) (which is protonated at values of pH lower than its pK_a of $\sim$10.6[29]) and establish the link between the rheological and morphological properties of the resulting interfacial gel. We demonstrate that modulation of OCNF surface charge, *via* tuning of ionic strength in the aqueous phase, leads to interfacial gels *via* adsorption and interfibrillar interactions. This work has implications for, for example, single-step fabrication of capsules with tailored shell properties, offering opportunities for fine control of mechanical properties.

Materials and methods

OCNF, prepared by TEMPO/NaOCl/NaBr oxidation[30] of wood pulp followed by high-pressure homogenization, were provided by Croda® International Plc (Goole, UK) as an 8 wt% slurry and purified as previously described[16] to achieve stable OCNF dispersions. The degree of oxidation of the OCNF (as the % of primary C6 hydroxyl groups oxidised to carboxylate groups) was measured to be 25% by conductometric titration.[31] Ultrapure DI water (18 MΩ cm) and hexadecane oil (Sigma-Aldrich®, 99%) were used, respectively, as the water and oil phases, except where stated otherwise. An OA stock solution (30 mM) was prepared by dissolving OA (Sigma-Aldrich®, primary amine >98%) in the oil and was subsequently diluted to yield a 4.25 mM OA in oil solution (above the herein reported critical micellar concentration (CMC) value of ≅2.7 mM (Fig. S1, ESI†), in close agreement with the previously reported value of ≅3.7 mM calculated for OA dissolved in Miglyol® 812 oil).[32] OA is almost insoluble in the aqueous phase. A 100 ppm OCNF dispersion was prepared by dilution of a 1 wt% OCNF in DI water dispersion, vortexed thoroughly and degassed using a bath sonicator (10 min). The OCNF concentration in water was chosen to ensure low viscosity of the aqueous phase, yet to provide a quantity of OCNF much greater than that required to saturate the O/W interface with an OCNF monolayer (calculation for the interfacial shear rheology experiments can be found in the ESI†). The 100 ppm OCNF dispersion and the 4.25 mM OA solution were used throughout, except where stated otherwise.

The interfacial properties of the OCNF–OA complex were measured using a stress-controlled rheometer (Discovery HR-3, TA Instruments®) at 25 °C equipped with a double wall ring (DWR) and a Couette cell geometry, following previously described methodology.[33,34] After loading of the aqueous phase into the cell (18.2 mL), the DWR was carefully positioned at the water/air interface. Briefly, the DWR was lowered to the water interface while measuring the axial force (N) as a function of distance. The distance corresponding to the water-DWR first contact was obtained by the drop in axial force (example provided in the Fig. S2, ESI†). The DWR was further immersed into the water phase by 500 μm, corresponding to 1/2 of the DWR thickness (calculated from the distance corresponding to the water-DWR first contact), to achieve accurate positioning of the DWR across the two phases (W/A). The oil phase (6 mL) was then gently added onto the water phase and, after 5 min allowed for equilibration, OA stock solution (30 mM) was added in order to reach a final OA concentration of 4.25 mM in the oil phase. The system was immediately subjected to the following sequence of experiments (Fig. 1): (TS1) 3 h time sweep at 1 rad s^{-1} angular frequency and 0.5% strain (γ_0); (SSC1) strain sweep cycle composed of two separate strain sweeps (0.05–100 γ_0(%)) at 1 rad s^{-1} separated by a 1 min rest time; (TS2) time sweep as in TS1; and, (SSC2) strain sweep cycle as in SSC1. The SSC1 and SSC2 segments were employed to induce a controlled breakage of the interfacial gel. When *in situ* NaCl solution injection was performed, an adapted Couette cell geometry (picture provided in the Fig. S3, ESI†) and a customized syringe pump (KD Scientific®), were employed, allowing the coupled injection and withdrawal of water phase at a constant rate of 0.1 mL min^{-1} thus maintaining the positioning of the DWR at the W/O interface. Specifically, the 100 ppm OCNF suspension was aged for 0.3 h below the OA-doped oil phase and following this an NaCl solution was added into the bottom of the aqueous phase to reach the final concentration of 55 mM. ζ-Potential measurements were conducted using a Malvern

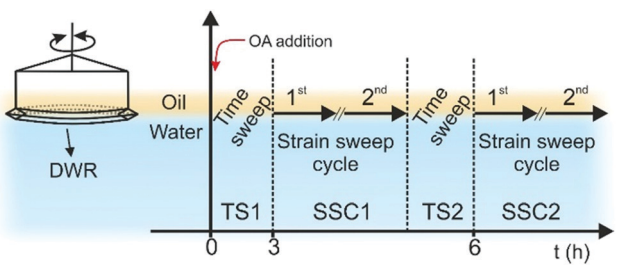

Fig. 1 Sketch of the double wall ring (DWR) at the W/O interface and the experimental sequences employed for the rheological study of the structures evolving at the W/O interface. TS1 and TS2 are time sweeps whilst, SSC1 and SSC2 are strain sweep cycles.

Zetasizer Nano ZSP® (Malvern, UK). Samples of OCNF 100 ppm dispersion in water at specific NaCl concentrations were placed in the capillary electrode cell and the ζ-potentials measured as an average of 4 measurements from 100 scans each. Macroscopic observation of formed interfacial gels was conducted after immersion of an OCNF-containing water droplet (10 μL) into 2 mL of OA-doped oil in a quartz cuvette (1 × 1 cm). Prior to imaging (USB camera equipped with a Kowa® LM75JC objective), the droplets were aged for *ca.* 24 h (at 25 °C) followed by gentle tilting.

To image the W/O interface using conventional optical microscopy (Brunel Ltd SP200 equipped with a Canon EOS 1300D), the water phase was loaded into 1 mm thick quartz cells, filling 2/3 of the volume, followed by gentle addition of the oil phase into the remaining 1/3 followed by aging in a vertical position for *ca.* 24 h (at 25 °C). The cell was then placed parallel to the focal plane of the microscope (rotation through 90°) and the interface imaged.

Confocal laser scanning microscopy (CLSM) analysis was performed at room temperature on a Zeiss LSM880 microscope (Zeiss, Germany). The oil phase was dyed with 0.1 wt% Nile Red (Sigma-Aldrich®): dye was added to the oil phase dispersed with stirring for 1 h and insoluble residues removed *via* centrifugation before OA was added to give a final concentration of 4.25 mM. In the case of double staining, the 100 ppm OCNF dispersion in 25 mM aqueous NaCl was prepared with Na-Fluorescein (Sigma-Aldrich®) added to a final concentration of 1 μM. The water droplets (10 μL) were aged for 24 h (at 25 °C) in the stained OA-doped oil. Prior to imaging, the water droplets, including shells, were pipetted onto a confocal microscope slide (25.4 × 76.2 mm) and covered with a coverslip.

To visualize the W/O interface using scanning electron microscopy (SEM, JEOL JSM6480LV, USA; at an operating voltage of 10 kV), styrene (Sigma-Aldrich®, 99%) was employed as the oil phase and polymerised using a modified protocol after Perrin *et al.*[35] In brief, prior to use, the styrene was passed through an inhibitor remover column and loaded with 1 wt% of a radical initiator (azobisisobutyronitrile, Sigma-Aldrich®) and pure OA to obtain a 4.25 mM OA solution, except where stated otherwise. The aqueous phase (1.5 mL) was loaded into a standing plastic syringe (NORM-JECT®, internal diameter 12.45 mm) followed by addition of 1.5 mL of the OA-doped styrene solution (gently placed on top of the water phase). The W/styrene interface was aged for 24 h and then the syringe placed into a pre-heated oven (55 °C for 24 h) to effect styrene polymerisation. After polymerisation, the polymerised styrene (polystyrene) was sliced, washed thoroughly with DI water, mounted on adhesive carbon tape and gold sputter-coated, prior to imaging.

Surface tension (γ) of the oil/air interface was measured using a surface tensiometer (Kibron, Ez-Pi+) equipped with a Dyne probe and γ determined as an average of 4 measurements of duplicate samples. The oil phase was titrated with an OA stock solution (30 mM) and allowed to equilibrate for 15 min, ensuring a time independent γ. The CMC was estimated as the point of change in slope of the domains above and below the CMC (Fig. S1, ESI†).

Results and discussion

Examination of the interfacial rheological behaviour of OCNF dispersions showed pronounced adsorption at the W/O interface and interfacial gel formation only when coupled with OA in the oil phase. Tuning of OCNF charge screening was found to be a key parameter, allowing enhancement of interfibrillar interactions at the W/O interface up to a point, where suppression of OCNF interfacial adsorption occurs.

Interfacial shear rheology

To probe the formation of the interfacial gel at the W/O interface with time (TS1), as well as the rheological response upon strain-induced breakage (SSC1) followed by recovery (TS2), *in situ* oscillatory rheology was conducted. Since fluid–fluid interfaces are governed by the contribution of both interfacial and bulk phenomena we ensured that the rheological measurements performed at the W/O interface effectively capture interfacial phenomena only (see ESI† for estimation of the bulk contribution to the interfacial rheology).

At first, the rheological properties of the separated components were investigated over time (TS1). When only OA was present, spontaneous adsorption of the amphiphilic OA at the W/O interface occured,[32,36] although values of the interfacial complex modulus ($|G_i^*|$) are below the limit of detectability of the instrument (Fig. 2a). Similarly, the sample containing only 100 ppm OCNF, in the absence of OA in the oil phase, did not show any structuring of the interface over 3 h, with values of $|G_i^*|$ of the order of 10^{-5}–10^{-4} Pa m (Fig. S4, ESI†). When OA in the oil phase was coupled with 100 ppm OCNF in the aqueous phase, a remarkable increase of $|G_i^*|$ occurred (Fig. 2a), as expected if there is a strong charge-driven adsorption of the negatively-charged OCNF onto the positively-charged W/O interface (induced by the positively-charged head group of OA; NH_3^+ for values of pH < pK_a of OAH^+, which is ~10.6[29]). Bertsch *et al.* reported that for unmodified CNC, a diffusion limited time lag is observed before adsorption occurrs,[15] whilst, similarly to the results herein described, Scheuble *et al.* showed that the kinetic of adsorption for methylated CNP is not delayed by a time lag.[21] This suggests that CNP hydrophobization or interfacial polyelectrolyte–CNP charge complexation (as herein described) are effective strategies to decrease the energy barrier for CNP adsorption at the W/O interface.[37]

The W/O interface behaved elastically, as denoted by the $\tan(\delta_i) = G_i''/G_i' < 1$ (Fig. 2b), with $G_i' > G_i''$ suggesting rapid formation of an elastic-like structure at the interface (G_i' being the interfacial storage modulus and G_i'' the interfacial loss modulus). The samples containing 100 ppm OCNF plus NaCl at 25 and 55 mM gave the largest values for $|G_i^*|$ and the lowest values of $\tan(\delta_i)$, indicating that, at these NaCl concentrations, stronger and more elastic interfacial gels formed. At even higher NaCl concentrations, 130 and 250 mM, the weakly structured interfaces point to a less favourable adsorption of OCNF at the W/O interface. This phenomenon is supported by the strong charge screening of OCNF (ζ-potential above −30 mV) at high NaCl concentrations where the electrostatic forces,

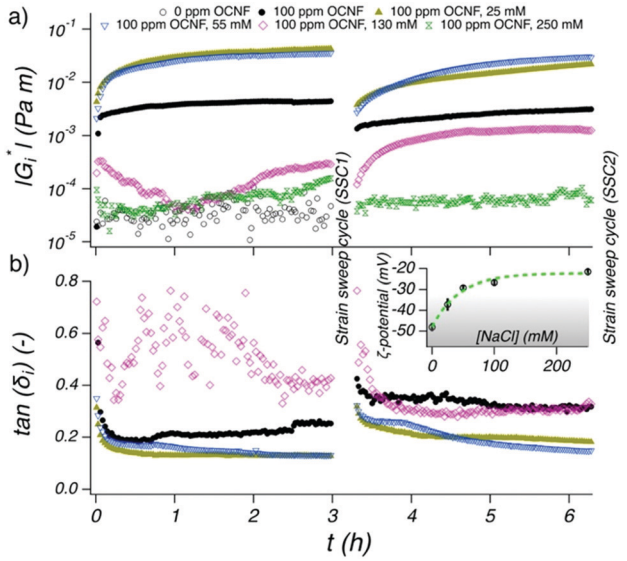

Fig. 2 Evolution of (a) $|G_i^*|$ and (b) $\tan(\delta_i)$ at the W/O interface composed of a OA-doped oil phase and a water phase containing 100 ppm OCNF with 0, 25, 55, 130 and 250 mM NaCl (0 ppm OCNF was used as a control sample). Measurements taken during TS1 and TS2 are displayed on the left and right respectively. ζ-Potential measurements of 100 ppm OCNF suspensions as a function of NaCl concentration, are shown in the inset. The grey shaded region denotes the ζ-potential regime where the repulsive electrostatic forces between fibrils outweigh the attractive forces and a line is drawn to guide the eye.

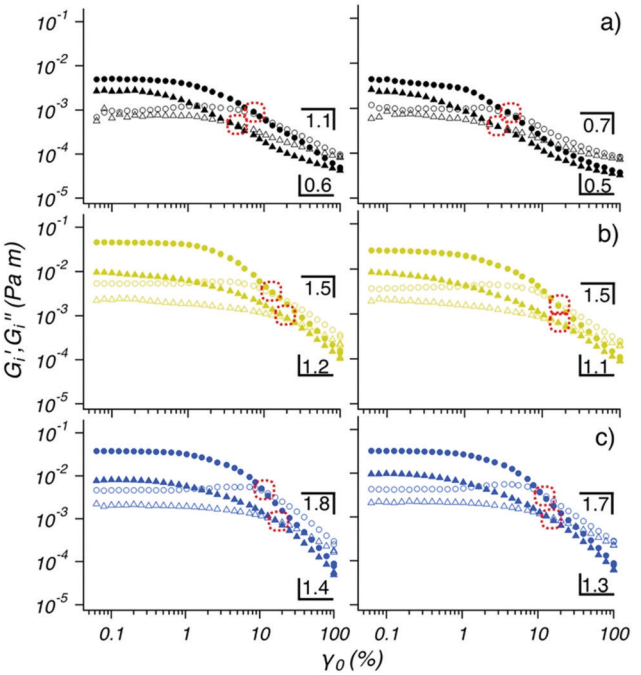

Fig. 3 Measurements conducted during SSC1 (left) and SSC2 (right) segments at the W/O interface for an aqueous phase containing 100 ppm OCNF in (a) 0, (b) 25 and (c) 55 mM NaCl solutions and an OA-doped oil phase. G_i' and G_i'' displayed as filled and empty symbols respectively. Circles and triangles indicate the first and second strain sweep, respectively. Dotted red circles show the yield point ($G_i' = G_i''$). The slope of the fitted G_i' power law decay ($R^2 > 97\%$), at large amplitude strains (10–100γ_0 (%)), is given for the first (above the data) and second (below the data) strain sweep.

the driving factor for the OCNF adsorption at the W/O interface, are outweighed by forces such as van der Waals and hydrogen bonds (inset Fig. 2b, see Fig. S5 (ESI†) for Debye length as function of NaCl concentration). Charge-driven polyelectrolyte assembly across W/O interfaces has previously been shown to have an increased surface tension, γ, with increasing ionic strength, indicating that co-adsorption of the polyelectrolytes decreases with increased charge screening.[22]

The rheological properties of the interface reached equilibrium ($|G_i^*|$ plateau) for the 100 ppm OCNF suspensions in the presence of 0, 25 and 55 mM NaCl within 3 h, indicating that both adsorption and rearrangement of OCNF at the W/O interface was complete within this time. After breakage of the structured interface, using a cycle of two oscillatory amplitude sweeps (SSC1), its recovery was followed (TS2). It is important to note that during the TS2 segment, the OCNF are already adsorbed at the interface (contrary to the TS1 segment), hence, the evolution of $|G_i^*|$ can be assigned solely to OCNF rearrangement across the W/O interface after disruption (assuming that the W/O surface area is constant). After breakage, the W/O interface formed in presence of 100 ppm OCNF at 0, 25 and 55 mM NaCl almost fully recovered their initial structure within 3 h, due to the reversible physical forces driving interfibrillar interactions. However, the 100 ppm OCNF at 130 mM NaCl, showed an increase in $|G_i^*|$ in the second sweep compared to the first sweep, suggesting incomplete OCNF adsorption within the first 3h of aging (during TS1). The strain sweep cycles (SSC1 and SSC2), composed of two amplitude sweeps separated by a 1 min resting time, were used to induce breakage of the structured interface and to allow extraction of information regarding the structural properties of the interface (Fig. 3). The samples at 0, 25 and 55 mM of NaCl showed $G_i' > G_i''$ at low strains ($\gamma_0 < 1\%$) and $G_i' < G_i''$ at larger strains; characteristic features of a gel-like structure, which behave as solids that yield and flow at higher strain values (illustrated for the strain sweep cycle of 100 ppm OCNF at 130 and 250 mM NaCl in Fig. S6, ESI†). This information, coupled with the film observed at the W/O interface presented in Fig. 6 suggest the gel-like nature of the interface.

In the SSC1 and SSC2 measurements, the moduli were observed to shift to lower values during the second amplitude sweep, which indicated incomplete network regeneration within the short 1 min resting period between the two amplitude sweeps.

This was expected as the previously described time sweeps showed that longer times are needed (>1 h) to achieve a complete recovery of the interfacial gel properties (Fig. 2).

The interfacial gels were compared at large strains (10–100γ_0(%)) where G_i' follows a power law scaling behaviour, $G_i'(\gamma_0) \propto {\gamma_0}^{-\mu}$, with the exponent μ being the slope. The weakly-structured interfacial gel formed by the 100 ppm OCNF suspension without salt was marked by a shallow μ (1.1) and by a yield strain, (chosen here as the strain value at which $G_i' = G_i''$) shifting toward lower values of strain with the second

amplitude sweep. On the other hand, the gel layers formed by a 100 ppm OCNF suspension at 25 and 55 mM NaCl exhibited tougher and stronger interfacial gels, as displayed by greater moduli and yield strain, respectively, and as expected for a firm interface, gave a greater value of μ (1.5 and 1.8 for 25 and 55 mM NaCl, respectively) indicative of a more abrupt breakage of the network. The yield strain associated with the second amplitude sweep, for both 25 and 55 mM NaCl, shifts toward larger values due to the fast regeneration of the interfacial properties. The SSC2 segment, performed after TS2, showed very similar features to the SSC1 segment, indicating that, especially for the 100 ppm OCNF suspension at 25 and 55 mM, interfacial structure was fully recovered.

To understand how electrostatic interactions affect the interfacial gel properties, an increase in ionic strength was induced after the initial formation of an interfacial gel prepared with 100 ppm OCNF in pure water *via* subsequent addition of NaCl solution to the subphase (Fig. 4a), thus allowing for charge screening of the OCNF only after initial OCNF adsorption at the W/O interface. Injection of the NaCl solution was made into the base of the cell, without stirring, to avoid disturbance to the interfacial region, meaning that some time was required for the ions to diffuse to the interface. Approximately 0.5 h after the NaCl injection, $|G_i^*|$ increased significantly while $\tan(\delta_i)$, after an overshoot, decreased, demonstrating that the interfacial gel became stronger (higher G_i') and more elastic (smaller G_i''/G_i' ratio) upon NaCl addition. The effect of ionic strength on the bulk rheology of OCNF dispersions has been widely exploited and charge screening effects have been associated with shorter interfibrillar distances leading to greater aggregation and gel formation.[3,12] A similar conclusion was suggested for the polyelectrolyte–CNC system investigated by Wu *et al.* who reported densification of the CNC interfacial layers across the W/O interface upon protonation of the sulfate groups.[38] For unmodified CNC across the W/A interface, a similar gain in viscoelasticity has been observed upon increase of ionic strength, in good agreement with the interfacial rheology described herein which strongly suggests enhanced interfibrillar aggregation at the W/O interface upon NaCl addition.[39]

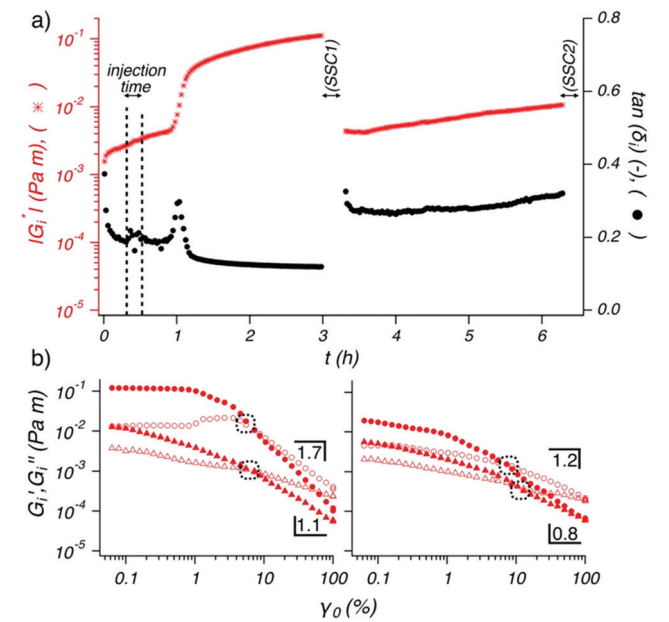

Fig. 4 Evolution of (a) $|G_i^*|$, in red, and $\tan(\delta_i)$, in black, at the W/O interface of an aqueous phase containing 100 ppm OCNF and OA-doped oil phase. At 0.3 h, an injection of NaCl solution was conducted over 10 min (indicated by dotted lines) to yield a final concentration of 55 mM NaCl in the aqueous phase. (b) G_i' and G_i'' are displayed as filled and empty symbols respectively, for the (left) SSC1 and (right) SSC2. Circles and triangles indicate the first and second strain sweep, respectively. Dotted circles show the yield point ($G_i' = G_i''$). The slope of the G_i' power law decay ($R^2 > 99\%$), at large strains (10–100γ_0 (%)), is given for the first and second strain sweep above and below the data, respectively.

Following the previously described protocol, SSC1 and SSC2 segments were performed interposed by TS2 (Fig. 4b). The first strain sweep in SSC1 showed values of G_i' greater than any other interfacial gel aged in presence of NaCl (from time = 0 h), and, the presence of a slight overshoot in G_i'' (before the moduli crossover) indicating that the interfacial gel yields plastically, a phenomenon which is usually associated with an interconnected network structure.[40,41] The effective disruption of the network at larger strain was highlighted by a value of μ = 1.7 and by a second amplitude sweep which did not recover a linear domain at low value of strains ($\gamma_0 < 1\%$). The moduli measured in the SSC2 segment performed after TS2 (Fig. 4b (right)) highlighted the limited recoverability of the interfacial structure even after TS2, where no linear domain was observed.

Morphology

The OA-OCNF complexation, at the macroscopic level, was investigated for different concentrations of NaCl in the aqueous phase (Fig. 5a). Droplets of the 100 ppm OCNF suspension in water at different NaCl concentrations were aged for *ca.* 24 h in an OA-doped oil solution and imaged after gentle tilting of the droplet. A 'hairy' structure at the W/O interface is weakly visible at 0 mM, while a pronounced folded interfacial layer, which is easily peeled off by gentle tilting of the droplets, appears at 25 and 55 mM NaCl. On the contrary, no substantial shell formation appeared for the droplets containing OCNF at 130 and 250 mM NaCl, in agreement with rheological results which showed stronger W/O interfaces at 25 and 55 mM NaCl. The macroscopic droplet shape however appears to be driven by the effects of OA and NaCl on interfacial tension since the droplets have similar shapes in the presence and absence of OCNF (for images see Fig. S7, ESI†).

The W/O interface of the 100 ppm OCNF suspension at 25 mM NaCl was analysed *via* optical microscopy by placing the two phases in a thin cuvette cell, as sketched in Fig. 5b, and imaged after *ca.* 24 h aging. In this case, the undisturbed interfacial gel showed a dendritic structure covering the whole layer formed at the W/O interface. A similar structure was present for the sample at 55 mM NaCl, although the structure appeared to be significantly less dense (for images of samples at other NaCl concentrations see Fig. S8, ESI†).

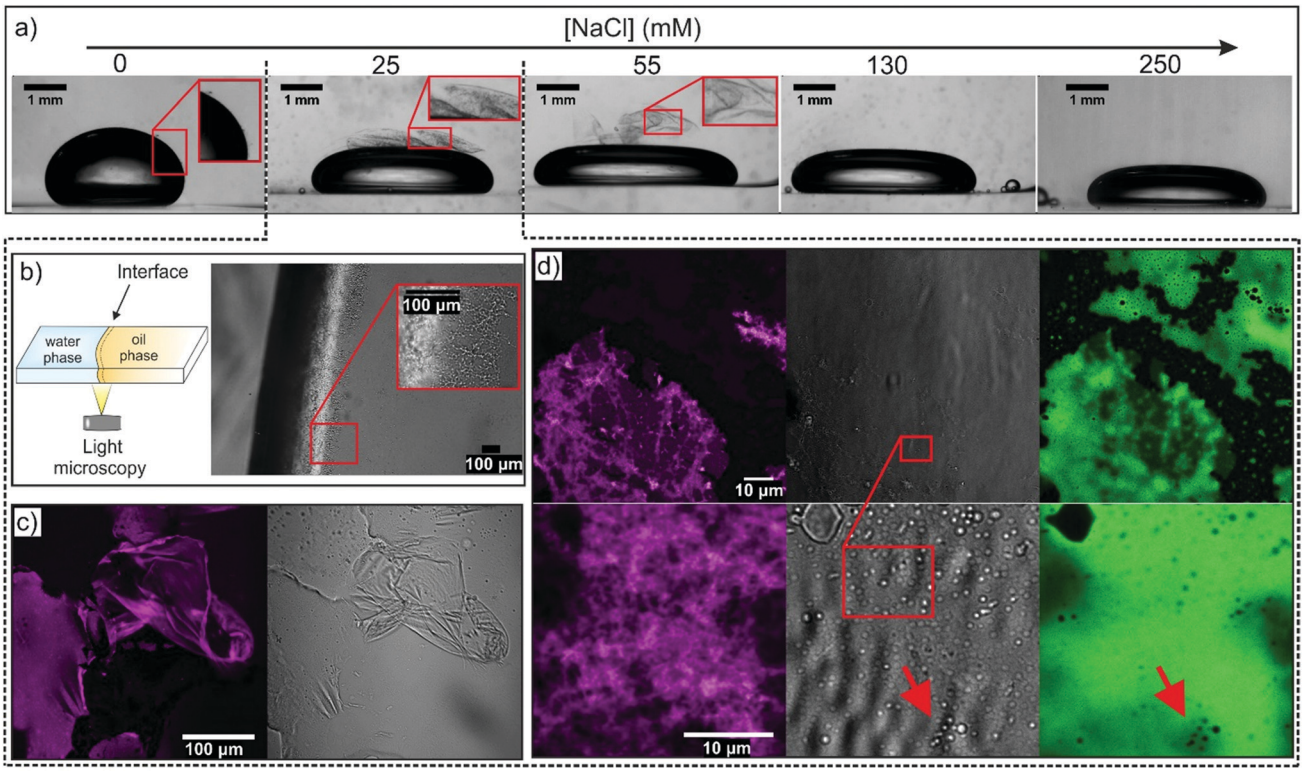

Fig. 5 (a) Images of 24 h aged OCNF-containing water droplets in OA-doped oil containing 100 ppm OCNF at various NaCl concentrations. (b) Optical micrograph of an undisturbed W/O interface between 100 ppm OCNF in 25 mM aqueous NaCl and OA-doped oil. The W/O interface was formed in a thin cuvette cell as depicted schematically. (c) CLSM images of the interfacial gel formed at the interface between 100 ppm OCNF in 25 mM aqueous NaCl and OA-doped oil; excitation channel for the oil-soluble dye (Nile red, depicted in magenta) and transmitted light displayed on the left and right respectively. (d) CLSM images at higher magnification collected with both oil-soluble and water-soluble dye (Na-Fluorescein, shown in green) for the sample as in (c); excitation channel for the oil-soluble dye, transmitted light and excitation channel for the water-soluble dye displayed on the left, centre and right respectively.

The interfacial gel morphology produced from a 100 ppm OCNF suspension in 25 mM aqueous NaCl was probed by CLSM using oil soluble Nile Red (Fig. 5c). The structure of the interfacial layer, at this magnification, displays wrinkles and sharp cuts, caused by the disruptive sample preparation. The gel resembled a shell-like structure, similar to the microcapsule shells produced by polyelectrolyte–nanoparticle complexation reported by Kaufman *et al.*[42] Homogeneous staining of the interfacial gel (shown in magenta, Fig. 5c) confirmed the presence of embedded oil. Surprisingly, at higher magnifications (Fig. 5d), a layer of jammed droplets was visible in the gel, similarly to that observed by Huang *et al.* employing nanoparticle-surfactant complexes (see ESI of Huang *et al.*).[43] The image of the film containing both the water-soluble dye, Na-Fluorescein, and the oil-soluble Nile Red showed that the droplets observed in the transmitted light configuration were not visible in the Nile red excitation channel, whilst non-fluorescent droplets were visible in the Na-Fluorescein excitation channel, indicating that the embedded droplets were oil-rich. Droplets of similar size are seen in the interfacial gels formed at 50 mM aqueous NaCl (shown in Fig. S9, ESI†). We also note that the number of droplets in the interfacial gel initially grows over time and a few hours are required to achieve saturation of the interfacial gel with oil droplets as observed in Fig. 5 and in Fig. 6b. After 24 h ageing, the W/O interface did not display substantial changes. Samples aged for several weeks also showed unchanged features, as visualized using confocal microscopy, suggesting that the embedded droplets are stable against coalescence.

To demonstrate the presence of oil-rich droplets within the interfacial layer, SEM analysis of the W/polystyrene interface was conducted for interfacial gels formed at 100 ppm OCNF and varying NaCl concentrations (Fig. 6). Since a different organic phase is used in this experiment, interface morphology was solely evaluated to observe the presence or absence of droplets at the interface, with the aim to further validate the CLSM observation. Flocs of droplets appeared at a low density across the entire W/polystyrene interface at 0 mM NaCl whilst at 25 mM NaCl, the droplets densely populated the interface, protruding into the aqueous phase. Surprisingly, higher magnification of the floc-free areas clearly revealed an interfacial layer of jammed droplets, analogous to the CLSM images. At 55 mM NaCl, the W/polystyrene interface showed an absence of flocs, although a "textured pattern" appeared, different from the smooth interface obtained from the control samples (W/OA-doped polystyrene,

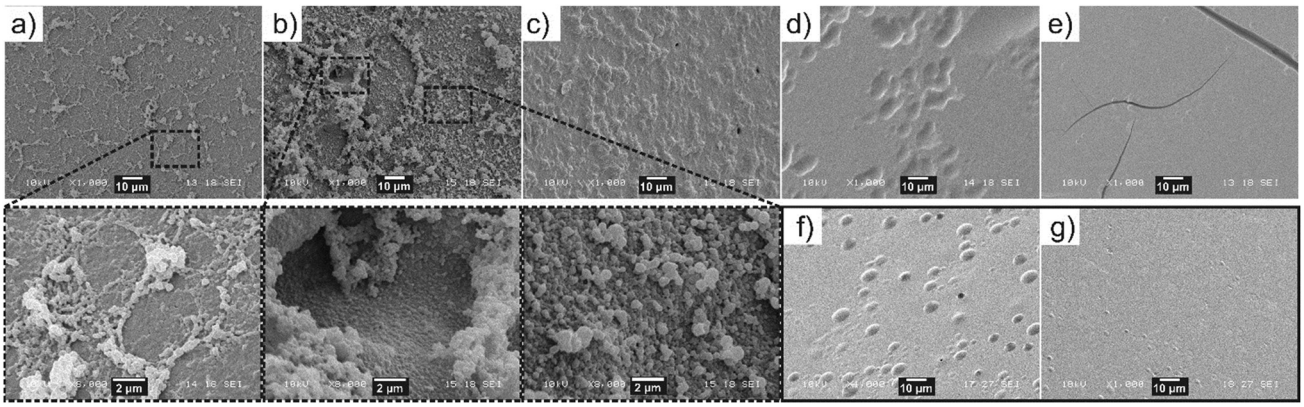

Fig. 6 SEM images of W/polystyrene interface from the aqueous "side", normal to the oil phase. The water phase was composed of 100 ppm OCNF at (a) 0, (b) 25, (c) 55, (d) 130 and (e) 250 mM NaCl, while the oil phase (polystyrene) was OA-doped. Control samples are (f) W/OA-doped polystyrene, in the absence of OCNF and (g) water-OCNF/polystyrene in the absence of OA. Zoomed areas are indicated by black rectangles.

in absence of OCNF (Fig. 6f), and water-OCNF/polystyrene in absence of OA (Fig. 6g)).

This suggests that at 55 mM, the interfacial gel at the W/polystyrene interface did not withstand the procedure required to induce polymerisation of the styrene (*i.e.*, heating and slicing of the polystyrene). However, at the highest NaCl concentrations, 130 and 250 mM, the W/polystyrene interfaces are as featureless as the control samples, indicating that, at these NaCl concentrations, there is no appreciable development of the droplet containing interfacial gel. The formation of oil-rich droplets at the W/O interface, observed at low NaCl concentrations, suggests that spontaneous emulsification occurs.[44] Similar phenomena have been recently observed for other oil-soluble surfactants across W/O interfaces.[40,45] This phenomenon is associated with a drastic decrease in γ, compensating for the increase in surface area associated with droplet formation, which favours negative Gibbs free energy values leading to spontaneous droplet formation.[44] It is possible, qualitatively, to relate both γ and $|G_i^*|$ to the particle volume fractions at the interface (ϕ_i) as $\gamma \propto 1/\phi_i$ and, $|G_i^*| \propto \phi_i$. This implies that $\gamma \propto 1/|G_i^*|$, indicating that the greatest values of $|G_i^*|$ for OCNF–OA complexes are concurrent with a strong decrease in γ, a prerequisite for spontaneous emulsification to occur. It is worth noting that the spontaneous formation of an oil-in-water emulsion across the interface also suggests that the OCNF–OA complexes have a three-phase contact angle $<90^\circ$, implying a favourable partitioning of the OCNF–OA complex into the water phase.[46] As such, we propose that the OCNF adsorption is essential for inducing self-emulsification, as well as stabilization of the oil-rich droplet at the interface. Specifically, the stabilization of the oil droplets within the interfacial gel suggests that the OCNF–OA complexes adsorb at the W/O interface of the oil droplets, acting as a physical barrier against coalescence, as previously reported for CNP in the context of Pickering emulsions.[13] Moreover, the interfacial gel across the planar W/O interface would allow droplet entrapment and bridging as shown by CLSM. On this basis, we suggest that the 2D assembly of OCNF across the W/O interface exists in three different regimes defined by the ζ-potential of OCNF particles (Fig. 7, top): (a) at ζ-potential more negative than -30 mV (0 mM NaCl), the highly negatively-charged OCNF spontaneously adsorbs to the W/O interface forming a weak interfacial gel due to complexation with the oppositely-charged OA; (b) at ζ-potential approximately equal to -30 mV (25 and 55 mM NaCl)

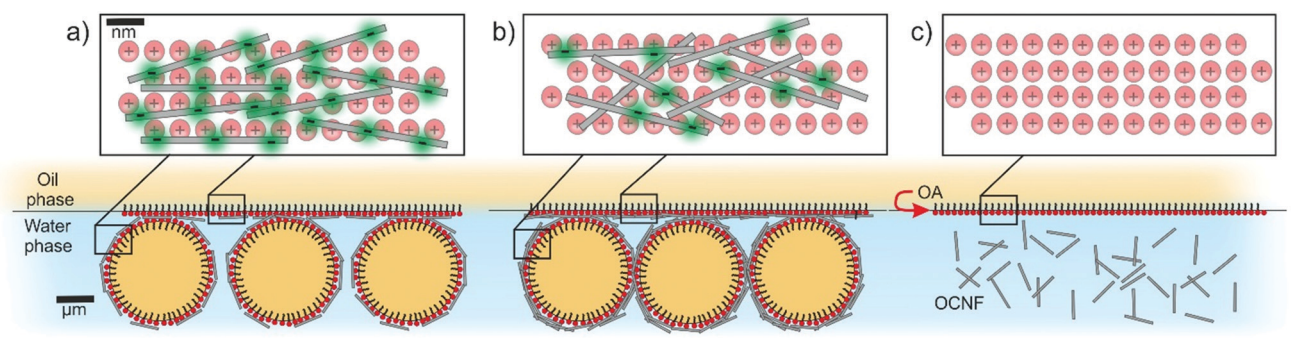

Fig. 7 (top) Schematic representation of the 2D OCNF–OA assembly (grey rectangles and red circle respectively, negative charges highlighted in green) across the W/O interface from a normal perspective upon three different regimes according to the NaCl concentration and thus the $|\zeta$-potential$|$ of the OCNF: (a) >30 mV, (b) ~ 30 mV and (c) <30 mV of the OCNF. (bottom) A zoomed-out representation from the parallel perspective. For clarity, components are not drawn to scale.

spontaneous OCNF adsorption at the W/O interface, coupled with some degree of charge screening, results in the formation of the strongest and toughest interfacial gels due to augmented interfibrillar interactions, and (c) at ζ-potential more positive than −30 mV (130 and 250 mM NaCl), little or no OCNF adsorption occurs, as the fibrils bear insufficient net charge to promote adsorption. At the micrometre length scale (Fig. 7, bottom), in the case of favourable OCNF adsorption, the interfacial gel embeds oil-rich droplets bridged by the salt-responsive OCNF.

Conclusions

The electrostatically-driven complexation of negatively-charged water-dispersible OCNF with positively-charged oil-soluble OA at W/O interface was investigated to elucidate the effect of ionic strength on OCNF adsorption and arrangement across the liquid–liquid interface. It was found that the ζ-potential of OCNF, modulated by changes in NaCl concentration, dictated OCNF adsorption and arrangement across the oppositely-charged W/O interface. Although absolute limits have yet to be established, the spontaneous formation of oil-rich droplets at the W/O interface suggests that spontaneous emulsification takes place upon OCNF–OA complexation. The utility of interfacial rheology combined with careful observation of 2D interfaces to discern the development of complex structures has been illustrated. The observations of interfacial gels embedding oil droplets, dependent on charge screening and adsorption to interfaces in bulk biphasic systems containing charged components, have implications for the production of hybrid gel-emulsion materials, capsule formation and tuning in O/W emulsions – systems where interfacial rheology studies are extremely challenging, yet where tuneability is key to utility.

Conflicts of interest

The authors declare no conflicts of interest.

Acknowledgements

The authors thank the EPRSC for funding this project (grant numbers EP/N033310/1). V. Calabrese thanks the University of Bath for PhD funding, Dr Andrea Pensado-Lopez for the useful discussions and Dr Giovanni Vorraro for the help provided in the customisation of the rheological apparatus. Data supporting this article have been made freely available *via* the University of Bath Research Data Archive system at DOI: 10.15125/BATH-00662.

References

1 S. J. Eichhorn, *Soft Matter*, 2011, **7**, 303–315.
2 T. Saito, T. Uematsu, S. Kimura, T. Enomae and A. Isogai, *Soft Matter*, 2011, **7**, 8804–8809.
3 H. Fukuzumi, R. Tanaka, T. Saito and A. Isogai, *Cellulose*, 2014, **21**, 1553–1559.
4 H. Dong, J. F. Snyder, K. S. Williams and J. W. Andzelm, *Biomacromolecules*, 2013, **14**, 3338–3345.
5 R. J. Crawford, K. J. Edler, S. Lindhoud, J. L. Scott and G. Unali, *Green Chem.*, 2012, **14**, 300–303.
6 N. Quennouz, S. M. Hashmi, H. S. Choi, J. W. Kim and C. O. Osuji, *Soft Matter*, 2015, **12**, 157–164.
7 V. Calabrese, J. C. Muñoz-García, J. Schmitt, M. A. da Silva, J. L. Scott, J. Angulo, Y. Z. Khimyak and K. J. Edler, *J. Colloid Interface Sci.*, 2019, **535**, 205–213.
8 K. J. De France, T. Hoare and E. D. Cranston, *Chem. Mater.*, 2017, **29**, 4609–4631.
9 D. da Silva Perez, S. Montanari and M. R. Vignon, *Biomacromolecules*, 2003, **4**, 1417–1425.
10 Y. Okita, T. Saito and A. Isogai, *Biomacromolecules*, 2010, **11**, 1696–1700.
11 S. Tsuguyuki and A. Isogai, *Biomacromolecules*, 2004, **5**, 1983–1989.
12 J. Schmitt, V. Calabrese, M. A. Da Silva, S. Lindhoud, V. Alfredsson, J. L. Scott and K. J. Edler, *Phys. Chem. Chem. Phys.*, 2018, **20**, 16012–16020.
13 I. Kalashnikova, H. Bizot, B. Cathala and I. Capron, *Langmuir*, 2011, **27**, 7471–7479.
14 V. Calabrese, J. C. Courtenay, K. J. Edler and J. L. Scott, *Curr. Opin. Green Sustainable Chem.*, 2018, **12**, 83–90.
15 P. Bertsch, M. Diener, J. Adamcik, N. Scheuble, T. Geue, R. Mezzenga and P. Fischer, *Langmuir*, 2018, **34**, 15195–15202.
16 V. Calabrese, M. A. Da Silva, J. Schmitt, J. C. Muñoz-Garcia, V. Gabrielli, J. L. Scott, J. Angulo, Y. Z. Khimyak and K. J. Edler, *Soft Matter*, 2018, **14**, 7793–7800.
17 N. Dhar, D. Au, R. C. Berry and K. C. Tam, *Colloids Surf., A*, 2012, **415**, 310–319.
18 Z. Hu, R. Xu, E. D. Cranston and R. H. Pelton, *Biomacromolecules*, 2016, **17**, 4095–4099.
19 M. E. H. van den Berg, S. Kuster, E. J. Windhab, L. M. C. Sagis and P. Fischer, *Phys. Fluids*, 2018, **30**, 072103.
20 M. E. H. van den Berg, S. Kuster, E. J. Windhab, J. Adamcik, R. Mezzenga, T. Geue, L. M. C. Sagis and P. Fischer, *Langmuir*, 2018, **34**, 10932–10942.
21 N. Scheuble, T. Geue, E. J. Windhab and P. Fischer, *Biomacromolecules*, 2014, **15**, 3139–3145.
22 H. Monteillet, F. Hagemans and J. Sprakel, *Soft Matter*, 2013, **9**, 11270.
23 H. Monteillet, J. M. Kleijn, J. Sprakel and F. A. M. Leermakers, *Adv. Colloid Interface Sci.*, 2017, **239**, 17–30.
24 M. Cui, T. Emrick and T. P. Russell, *Science*, 2013, **342**, 460–463.
25 Y. Chai, A. Lukito, Y. Jiang, P. D. Ashby and T. P. Russell, *Nano Lett.*, 2017, **17**, 6453–6457.
26 G. Kaufman, S. Mukhopadhyay, Y. Rokhlenko, S. Nejati, R. Boltyanskiy, Y. Choo, M. Loewenberg and C. O. Osuji, *Soft Matter*, 2017, **13**, 2733–2737.
27 X. Liu, S. Shi, Y. Li, J. Forth, D. Wang and T. P. Russell, *Angew. Chem., Int. Ed.*, 2017, **56**, 12594–12598.
28 S. Shi, X. Liu, Y. Li, X. Wu, D. Wang, J. Forth and T. P. Russell, *Adv. Mater.*, 2018, **30**, 1–5.

29 M. A. Scorciapino, R. Sanna, A. Ardu, F. Orr, M. Casu, A. Musinu and C. Cannas, *J. Colloid Interface Sci.*, 2013, **407**, 67–75.
30 T. Saito, Y. Nishiyama, J. L. Putaux, M. Vignon and A. Isogai, *Biomacromolecules*, 2006, **7**, 1687–1691.
31 T. Saito and A. Isogai, *Biomacromolecules*, 2004, **5**, 1983–1989.
32 N. G. Eskandar, S. Simovic and C. A. Prestidge, *Phys. Chem. Chem. Phys.*, 2007, **9**, 6313–6318.
33 A. Franck, *5th Int. Symp. Food Rheol.*, 1997, vol. 8, pp. 242–244.
34 S. Vandebril, A. Franck, G. G. Fuller, P. Moldenaers and J. Vermant, *Rheol. Acta*, 2010, **49**, 131–144.
35 E. Perrin, H. Bizot, B. Cathala and I. Capron, *Biomacromolecules*, 2014, **15**, 3766–3771.
36 W. Wu, H. Fang, F. Yang, S. Chen, X. Zhu, Q. Yuan and W. Gan, *J. Phys. Chem. C*, 2016, **120**, 6515–6523.
37 K. Du, E. Glogowski, T. Emrick, T. P. Russell and A. D. Dinsmore, *Langmuir*, 2010, **26**, 12518–12522.
38 X. Wu, Q. Yuan, S. Liu, S. Shi, T. P. Russell and D. Wang, *ACS Macro Lett.*, 2019, **8**, 512–518.
39 P. Bertsch and P. Fischer, *Langmuir*, 2019, **35**, 7937–7943.
40 S. Bochner De Araujo, M. Merola, D. Vlassopoulos and G. G. Fuller, *Langmuir*, 2017, **33**, 10501–10510.
41 L. M. C. Sagis and P. Fischer, *Curr. Opin. Colloid Interface Sci.*, 2014, **19**, 520–529.
42 G. Kaufman, S. Nejati, R. Sarfati, R. Boltyanskiy, M. Loewenberg, E. R. Dufresne and C. O. Osuji, *Soft Matter*, 2015, **11**, 7478–7482.
43 C. Huang, J. Forth, W. Wang, K. Hong, G. S. Smith, B. A. Helms and T. P. Russell, *Nat. Nanotechnol.*, 2017, **12**, 1060–1063.
44 C. Solans, D. Morales and M. Homs, *Curr. Opin. Colloid Interface Sci.*, 2016, **22**, 88–93.
45 P. S. Silva, S. Zhdanov, V. M. Starov and R. G. Holdich, *Colloids Surf., A*, 2017, **521**, 141–146.
46 B. P. Binks, L. Isa and A. T. Tyowua, *Langmuir*, 2013, **29**, 4923–4927.